Mechanical Hysteresis in Actin Networks: Supplementary information

Sayantan Majumdar, Louis C. Foucard, Alex J. Levine, and Margaret L. Gardel

Methods

Protein preparation

Monomeric actin (G-actin) was purified using protocol adapted from Ref.[1] from rabbit skeletal muscle acetone powder (Pel Freeze Biologicals, Product code: 41008-3). Small aliquots of actin solution were drop frozen in liquid nitrogen, and stored at -80 ^{o}C. For each experiment fresh aliquots of frozen actin were thawed and used. FLN was purified from chicken gizzard and aliquots were also stored at -80 ^{o}C.

In-vitro network formation

10X actin polymerization-buffer (2 mM TrisHCl, 2 mM $MgCl_2$, 100 mM KCl, 0.2 mM DTT, 0.2 mM $CaCl_2$, 0.5 mM ATP, pH 7.5) was mixed with freshly thawed FLN. Freshly thawed G-actin was mixed with 1X Ca-G-buffer (2mM Tris-HCl, 0.2mM ATP, 0.5mM DDT, 1mM NaN_2 and 0.1mM $CaCl_2$, pH 8). 1X Ca-G-buffer containing G-actin and 10X actin polymerization buffer containing FLN were mixed gently for 10 s just before loading the sample to initiate the polymerization process of actin filaments in the rheometer sample chamber.

Model

We developed a mathematical model of the system as a two-dimensional network of N semiflexible filaments with identical elastic properties and length L. To construct the numerical network, each filament is placed at random in a box of area A with an orientation picked from a distribution $P(\theta)$, where θ denotes the angle between the filament and the nematic director $\mathbf{n}$ of the network.

Network geometry

The geometry of the network is characterized by the scalar amplitude of the nematic order parameter S, found from the width of the distribution $P(\theta)$:

$$S = 2\int_0^\pi d\theta P(\theta)\cos(2\theta). \tag{1}$$

Our results are remarkably insensitive to the exact form of distribution of filament angles (Fig.S9).

We have been using the following distribution in our simulations:

$$P(\theta) = \frac{e^{\alpha\cos 2\theta}}{2\pi I_0(\alpha)} \tag{2}$$

where $I_0(\alpha)$ the modified Bessel function of the first kind of order 0. The parameter α is tied to the nematic angle and is found numerically by solving $S = I_1(\alpha)/I_0(\alpha)$.

Another geometric characteristic of the network is the mean distance between consecutive crosslinks along a given filament, l_c, which is inversely proportional to the network density and depends on the nematic order parameter S. This quantity is necessary to assess the propensity for buckling. Long spans between consecutive cross links buckle at a lower compressive stress than shorter ones. This quantity may be computed by considering a filament lying at an angle θ with respect to the nematic director. The probability of a second filament crossing at an angle ψ with respect to the first is given by $L^2|\sin\psi|/A$. In order to obtain the crossing probability independent of the relative angle ψ, we need to integrate the above quantity over ψ with a weight $P(\theta+\psi)$. Doing this gives:

$$P_{\rm cross}(\theta) = \frac{2L^2}{A}\int_0^\pi d\psi\,|\sin\psi|\,P(\theta+\psi) \tag{3}$$

This quantity is simply the probability that a given filament oriented with angle θ to the nematic direction is crossed by a second filament with its direction chosen from the angular probability distribution and its position chosen randomly. We will again assume that our system contains a large number of filaments N in a large area A, so that $P_{\rm cross}(\theta)$ is small; in this limit, the probability distribution $p_n(\theta)$ for the number of crosslinks on a filament oriented with angle θ to the nematic direction can be approximated by the following Poisson distribution:

$$p_n(\theta) = \frac{e^{-n_c(\theta)}[n_c(\theta)]^n}{n!} \tag{4}$$

where $n_c(\theta)$ is the mean number of cross links on a filament oriented with angle θ, and is written:

$$n_c(\theta) = 2\rho L^2\int_0^\pi d\psi\,|\sin\psi|\,P(\theta+\psi), \tag{5}$$

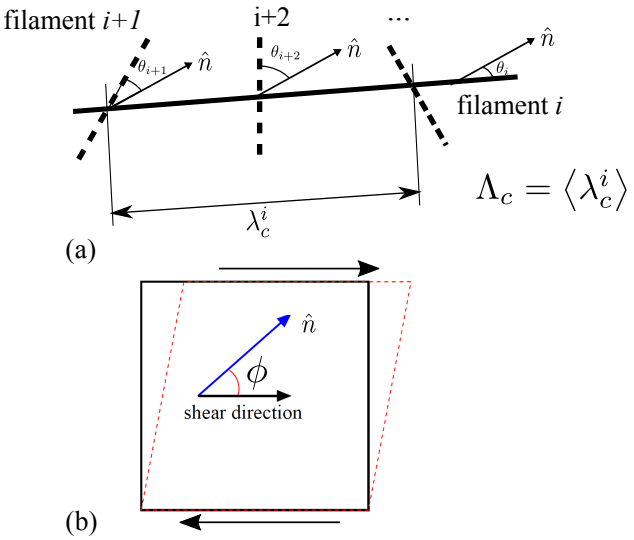

Figure M1 Geometric properties of the network. (a) Λ_c is the average (over filaments) of the distance λ_c^i between the two most distance crosslinks on a filament i. The orientation of filament i is defined as the angle θ_i made with the nematic director $\hat{n}$. (b) The nematic director $\hat{n}$, in turn, makes an angle ϕ with respect to the displacement direction of the applied shear (here the x axis).

with $\rho = N/A$ the filament density. We then calculate the distance Λ_c between the two most distant crosslinks (see Fig.M1) on a filament and the average number of intervals between two crosslinks on a filament N_c. These quantities are given by:

$$\Lambda_c = 2NL \int_0^\pi d\theta P(\theta) \sum_{n=0}^{\infty} p_n(\theta) \frac{n-1}{n+1} \tag{6}$$

$$N_c = 2N \int_0^\pi d\theta P(\theta) \sum_{n=2}^{\infty} p_n(\theta)(n-1) \tag{7}$$

Finally, the ratio of Λ_c and N_c yields the mean distance between crosslinks:

$$l_c = L \frac{1 + \langle e^{-n_c} \rangle - 2\left(\left\langle \frac{1}{n_c} \right\rangle - \left\langle \frac{e^{-n_c}}{n_c} \right\rangle \right)}{\langle n_c \rangle - (1 - \langle e^{-n_c} \rangle)}, \tag{8}$$

where $\langle \cdot \rangle$ denotes the averaging operation over θ with weight $P(\theta)$.

Experimental details

Bulk rheology

All rheological measurements were performed on a Bohlin Gemini HR Nano (Malvern Instruments) rheometer at a temperature of 25^0C, using a 40 mm diameter acrylic plate and 160 μm gap. The acrylic plate has much lower moment of inertia compared to a similar metal plate and hence rheological measurements are more robust under fast direction switching of the plate rotation. We confirmed results were independent of plate geometry (Fig.S8). We also used a humidity chamber sealed with vacuum grease to reduce water evaporation from the sample during the rheology experiments and observed that the sample's rheological properties were essentially unchanged for periods up to ~ 4 hours after loading the sample in the rheometer. The mechanomemory effect described in this manuscript is a robust effect, observed 100% of the time in > 35 independent samples.

After loading the sample, the build-up of linear elastic G' and viscous G'' moduli was measured as a function of time at a fixed frequency $f = 0.5$ Hz with a very small strain amplitude $\gamma_0 = 0.02$ (ensuring linear response) to monitor the polymerization process indicated by the increase in magnitude of G' and G'' with time. After approximately 1 hour, the moduli saturate indicating a fully polymerized starting state of cross-linked actin network. This state is the untrained state of the network. The tangent shear modulus $K(\gamma)$ is measured from the Lissajous plots (Fig.1d) by numerically calculating $\frac{\delta\sigma}{\delta\gamma}|_\gamma$ along the increasing strain magnitude under various training conditions. Memory is quantified by the asymmetry of tangent shear modulus ΔK in positive and negative direction at strain $|\gamma| = 0.4$, i.e. $\Delta K(|\gamma|) = K(+\gamma)$ - $K(-\gamma)$. The choice of this strain controls the absolute value of the strength of memory, but does not affect changes in memory due to training or our analysis. To estimate the error in ΔK, we first numerically fit a spline smoothing curve (averaged over 10 adjacent points) to K vs γ plot. Then we take the difference of this smooth curve from the raw data. The standard deviation (SD) of such differences gives the error in K. The error bars in ΔK are twice the standard deviations, since the uncertainty gets doubled when taking the difference. We consistently follow this method to estimate the error in ΔK.

To get the phase information, the complex tangent shear modulus $K^*(\sigma,\omega)$ was measured by superposing a small sinusoidal component of amplitude $\delta\sigma$ and angular frequency ω on a constant background stress σ with $\delta\sigma = 0.1\sigma$. Then we measured the amplitude of the sinusoidal strain $\delta\gamma$ at the same angular frequency ω and the phase difference Δ between the sinusoidal stress and the strain. The magnitude of the tangent shear modulus is given by $K(\sigma,\omega) = \frac{\delta\sigma}{\delta\gamma}|_\sigma$.

Under steady shear, $P = \sigma\dot{\gamma}$ gives the instantaneous injected power per unit volume. However, since the system is visco-elastic, some part of this injected energy is dissipated and some part is stored. When the training stress is switched off, the system can relax back partially using the stored energy. We can also get insight about the dissipation in the system by superposing a small amplitude sinusoidal component on top of the large D.C. stress component. By this method we can measure the phase difference between the applied sinusoidal stress and resulting sinusoidal strain. When we plot the sinusoidal strain vs sinusoidal stress over a complete cycle, we get a closed curve (Lissajous plot) that can be well approximated by an ellipse in our case. The area under the curve is proportional to the total dissipated energy over a complete cycle. Here, it should be clear that the dissipated energy will also depend on the amplitude and frequency of the applied sinusoidal signals. Thus, by this method we cannot estimate the absolute power dissipation. However, if we use the same amplitude and frequency of the input sinusoidal component, we can compare how the power dissipation occurs as a function of time during the creep behavior under D.C. stresses. The energy dissipated over a complete cycle is $E_{cycl} = \pi\delta\sigma\,\delta\gamma sin\Delta$, leading to an average instantaneous power dissipation of $P(t) = (\omega/2\pi)E_{cycl}$. We define $P_{\alpha\beta}(t)$ to be the average instantaneous power dissipation in the β direction in a sample trained in the α direction. Here α and β can assume only the values $\pm$. Under steady shear, we calculate the injected power and subtract out the recoverable power at every instant to estimate the time dependent power dissipation (Fig.S3). However, to do this one has to assume that the injected power at the start up of creep response corresponds to the recoverable power at the start of recovery curve.

Confocal microscopy

20% molar ratio of labeled actin monomers (actin from rabbit skeletal muscle conjugated with Alexa fluorophore 568, Life Technologies Corp., product part no. A12374) was added to 80% G-actin and then the combination is mixed gently with 1X Ca-G-buffer. Ca-G-buffer con-taining both labeled and unlabeled G-actin and 10X actin polymerization buffer containing FLN were mixed gently for 10 s just before loading the sample into a home built glass chamber (thickness $\sim 100\mu$m) mounted on the sample stage of a laser scanning confocal microscope (Nikon) with a 60X water immersion objective. Z-stack images were recorded approximately after 1 hour of polymerization.

Confocal imaging under shear

To observe the network structure under shear deformation, we made a home built transparent shear-cell that can be mounted on a confocal microscope. This shear-cell is composed of two parallel glass cover slips. The top cover slip is coupled to a position controlled micro-manipulator (Shutter Instrument) through a 3-D printed probe. The gap between the plates are maintained at 100μm using the z displacement of the micro-manipulator, after loading the sample. For applying shear deformations, the top plate is moved in x-y plane.

Detailed model

Simulation details

Using classical Bernoulli-Euler beam theory, the mechanical properties of the filaments are characterized by the linear stretching and bending moduli, μ and κ respectively. The elastic length scale or bending length $\lambda_b = \sqrt{\kappa/\mu}$ determines the relative contribution of the filament's bending and stretching modes to the total energy. The thermal persistence length of the filaments is given by $\ell = \kappa/k_{\mathrm{B}}T$. The energy of a single filament can then be written as,

$$E_{\mathrm{f}} = \int_L ds \left[\frac{\mu}{2} \left| \frac{d\mathbf{r}}{ds} \right|^2 + \frac{\kappa}{2} \left(\frac{d\theta}{ds} \right)^2 \right], \tag{9}$$

where we used an arclength parametrization of the filament with $\mathbf{r}(s)$ the position of the filament cross-section after deformation, and θ the rotation of the filament caused by that deformation. We consider a system composed of N semiflexible filaments connected together by cross links at points of intersection. We implement a mechanical model for the filamin cross links that is based on previous experimental measurements [Ref. (2)].The filamin contour length is $\sim$100 nm, but is comprised of subunits of rest length $\sim$10 nm that unfold under force. Previous experimental results show that, during unfolding, the subunits follow a worm-like chain model [Ref. (2)]. In the simulation, the saw-tooth force-extension curve is reduced to two regimes, reflecting the regime of subsequent unfolding and the nonlinear stiffening observed during stretching of the last segment. This was adopted in order to reduce problems arising from numerical instability. For lengths below 150 nm, the 1d spring constant is $\mu_{lc} = 100pN$. In the stiffening regime above $150nm$, there is a linear increase in the spring constant of 10 pN/nm for further extension. The cross links are extensible nonlinear elastic elements as described above, but they supply no constraint torques, being free to rotate. The filaments are spatially discretized by placing nodes at each cross link, as well as at regular intervals between adjacent cross links, which ensures a sufficient level of spatial refinement for numerical convergence. Typically, networks are generated with 4000 filaments discretized into 100 000 finite elements. The construction of each network is based on the two geometric parameters defined above: (a) the nematic order parameter S and (b) the mean filament density l_c. To build the network, we add filaments sequentially to the simulation box with typical dimensions of $A = 64L^2$. We numerically evaluate the strain energy using the discretized version of Eq. 1:

$$\tilde{\mathscr{H}} = \frac{\mu}{2} \sum_{\text{segments}} \frac{(d-d_0)^2}{d_0} + \kappa \sum_{\text{angles}} \frac{1-\cos\beta}{l_0}, \tag{10}$$

where d and d_0 are respectively the current and original length of the segments, and l_0 is the average rest length of two adjacent segments forming an angle β. The nematic order parameter is set by choosing the direction of the filaments from the distribution given in Eq. 3, with a width determined to give the desired nematic order parameter S. The centers of the mass of the filaments remain uniformly distributed during the construction of all networks. We have explored the mechanics of networks constructed using other

anisotropic orientational distributions of the filaments, and found only small changes in the collective mechanics of the networks when both the network density and nematic order parameter were held constant. See Fig.S9.

We use the Lees-Edward method [Ref. (3)]to simulate the shearing deformation of the network with periodic boundary conditions, and the static equilibrium of the system is obtained by energy relaxation using a quasi-Newton minimization algorithm [Ref.(4) and (5)].

From residual strain to nematic order

The residual strain measured after training implies a realignment of the filaments in the network. Assuming that the residual strain results from the affine deformation of a formerly isotropic network, we compute the nematic order parameter S induced by training. Choosing an arbitrary filament from an isotropic 2D network of filaments (length L), we write its initial orientation as

$$\mathbf{R} \quad = \quad L \begin{bmatrix} \cos\theta \\ \sin\theta \end{bmatrix} \tag{11}$$

with θ the angle made by the filament with respect to the x axis. We apply a simple shear along direction x in the xy plane. Under this deformation the filament rotates make the angle θ' with respect to the same x axis, given by

$$\mathbf{R}' \quad = \quad L \begin{bmatrix} \cos\theta + \gamma\sin\theta \\ \sin\theta \end{bmatrix} = L \begin{bmatrix} \cos\theta' \\ \sin\theta' \end{bmatrix}. \tag{12}$$

The new angle θ' is thus

$$\theta' \quad = \quad \arctan\left[\frac{\sin\theta}{\cos\theta + \gamma\sin\theta}\right]. \tag{13}$$

Considering the ensemble of filament orientations given by the unit vectors $\mathbf{u} = (\cos\theta, \sin\theta)$ in the isotropic network, we apply the mapping Eq. 13 to obtain the new (anisotropic) distribution $\mathbf{u}' = (\cos\theta', \sin\theta')$ of filament orientations after the shear deformation $\lambda = \delta + \gamma\mathbf{xy}$. From this distribution we directly compute the resulting nematic order parameter tensor by averaging over the initially isotropic distirbution of angles θ. Denoting this average by $\langle . \rangle$, we write the order parameter $S_{ij} = \left\langle u'_i u'_j \right\rangle - \frac{1}{2}\delta_{ij}$ as:

$$\begin{aligned} S_{11} \quad &= \quad \frac{\gamma^2+2}{\gamma^2+4} - \frac{1}{2}, \; S_{12} = S_{21} \; = \; \frac{\gamma}{\gamma^2+4} \\ S_{22} \quad &= \quad \frac{2}{\gamma^2+4} - \frac{1}{2}, \end{aligned} \tag{14}$$

Finally, after diagonalization, we find the magnitude of the order parameter S to be given by

$$S(\gamma_r) = \frac{\gamma_r}{\sqrt{\gamma_r^2+4}} \tag{15}$$

This provides an explicit expression for the nematic order as a function of the residual strain γ_r.

Mean field approach

We develop a mean field calculation of the shear modulus as a function of nematic order. We shear the network along the $+x$ direction, where the nematic director makes an angle ϕ with respect to x (Fig.M1b). We assume that filaments buckle only when under a compressive load larger than the Euler buckling load p_c, which depends on the length of the filament segment between consecutive cross links and on the angle that that filament makes with the shearing direction. We further assume that one may neglect the (small) amount of elastic energy stored in filaments post-buckling.

Under these assumptions, a filament oriented making an angle ψ with the x-axis has an energy per unit length

$$E_{\mathrm{f}}(\psi) = \mu\gamma^2\cos^2\psi\sin^2\psi/2, \tag{16}$$

if not buckled. Based on the Euler buckling criterion, there is a wedge of width $2\omega_{\mathrm{Euler}}(\ell)$ around the compression direction of the shear so that filament segments of length greater than ℓ oriented within this wedge will buckle. We wish to exclude such buckled filaments from the computation of the elastic energy stored in the network using Eq. 16. We replace this segment-length dependent quantity $2\omega_{\mathrm{Euler}}(\ell)$ with an averaged excluded wedge angle, θ_c. This is determined self-consistently by setting the average filament segment length (averaged only over the wedge of half angle θ_c) to be equal to the load-dependent critical length for Euler buckling $l_{\mathrm{buckle}}(\gamma)$. This results in a self-consistent integral equation to be solved for θ_c, and which depends on both the degree of nematic order and shear strain γ:

$$l(\theta_c) = L\frac{1 + \left\langle e^{-n_c}\right\rangle - 2\left(\left\langle \frac{1}{n_c}\right\rangle - \left\langle \frac{e^{-n_c}}{n_c}\right\rangle\right)}{\langle n_c\rangle - (1 - \langle e^{-n_c}\rangle)} = l_{\mathrm{buckle}}, \tag{17}$$

where $\langle\cdot\rangle$ notes denotes the average over the wedge for a given degree of nematic order $P(\theta)$. This is solved numerically.

We then compute the total network energy by integrating Eq. 16 over the filament orientation and length [Ref.(24) in the main text]excluding the wedge of half angle θ_c surrounding the compression direction, oriented along $\theta_{\rm comp}$= -45 degrees with respect to the shearing direction. The total energy of the network is

$$\begin{aligned} E(\phi) &= \mu\rho\gamma^2 \left(\int_0^{\theta_{\rm comp}-\theta_{\rm c}} \cos^2\psi \sin^2\psi/2 \right. \\ &\times \sum_{n=2}^{\infty} \frac{L(n-1)p_n(\psi-\phi)}{n+1} \\ &+ \int_{\theta_{\rm comp}+\theta_{\rm c}}^{\pi} \cos^2\psi \sin^2\psi/2 \\ &\times \left. \sum_{n=2}^{\infty} \frac{L(n-1)p_n(\psi-\phi)}{n+1} \right), \end{aligned} \tag{18}$$

Using the fact that $E(\phi) = K(\phi)\gamma^2/2$ for small shear, we write the tangent modulus as

$$\begin{aligned} K(\phi) &= 2\mu\rho \int_0^{\theta_{\rm comp}-\theta_{\rm c}} d\psi \left(\cos^2\psi \sin^2\psi/2 \right. \\ &\times \left. \sum_{n=2}^{\infty} \frac{L(n-1)p_n(\psi-\phi)}{n+1} \right) \\ &+ 2\mu\rho \int_{\theta_{\rm comp}+\theta_{\rm c}}^{\pi} d\psi \left(\cos^2\psi \sin^2\psi/2 \right. \\ &\times \left. \sum_{n=2}^{\infty} \frac{L(n-1)p_n(\psi-\phi)}{n+1} \right). \end{aligned} \tag{19}$$

The mean-field value of ΔK computed using Eq. 19 is shown in Fig.4d (main text) as a dashed black line. The mean-field model is consistent with both the simulation (red line and symbols) and the experiment (points).

Table 1 Table of parameters

Parameters	Symbol	magnitude	Ref.
(Geometrical)			
F-actin length	L	2 μm	Viamontes *et al.*, PRE, 2006 [Ref.(6)]
Average distance between cross-linking points		$\approx$ 80 nm	
Persitence length of filamin subunits		$\approx$ 1 nm	Xu *et al.*, Biophysical J., 2013 [Ref.(2)]
Nematic order	S	0-1	
Finament density		16 filaments / $(\mu m)^2$	
(Mechanical)			
F-actin bending mod.	κ	6.5×10^4 $pN.nm^2$	Yanagida et al., Nature, 1984
F-actin 1d modulus	μ	17.1 nN	Kojima et al., PNAS, 1994 [Ref.(7)]
F-actin Euler buckling force (L = 2 μm)		0.16 pN	Calculated using 'L' and 'κ' values

Notes and references

[1] J. Spudich and S. Watt, *J. Biol. Chem*, 1971, **246**, 4866–4871.

[2] T. Xu, H. Lannon, S. Wolf, F. Nakamura and J. Brujic, *Biophysical journal*, 2013, **104**, 2022–2030.

[3] A. Lees and S. Edwards, *Journal of Physics C: Solid State Physics*, 1972, **5**, 1921.

[4] R. H. Byrd, P. Lu, J. Nocedal and C. Zhu, *SIAM J Sci Comput*, 1994, **16**, 1190–208.

[5] C. Zhu, R. H. Byrd, P. Lu and J. Nocedal, *ACM Trans Math Softw*, 1994, **23**, 550–60.

[6] J. Viamontes, S. Narayanan, A. Sandy and J. Tang, *Physical Review E*, 2006, **73**, 1–10.

[7] H. Kojima, A. Ishijima and T. Yanagida, *Proceedings of the National Academy of Sciences of the United States of America*, 1994, **91**, 12962–6.

S.I. Figures

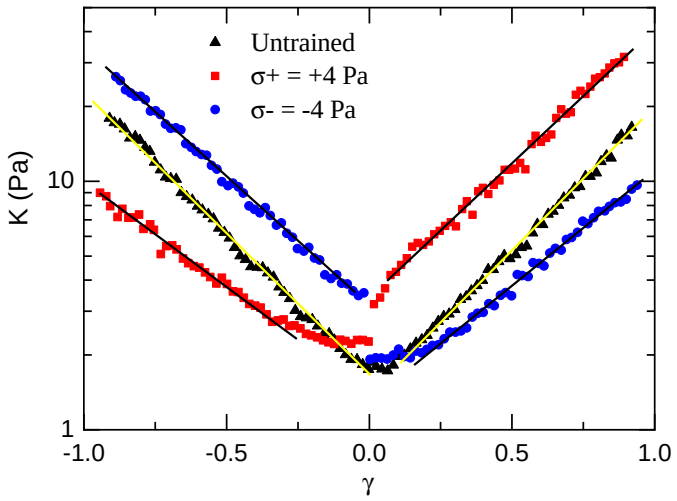

Figure S1 Log-linear plot showing exponential dependence of shear modulus (K) on strain, implying that K varies linearly with applied stress. Solid lines are guides to the eye. Here, c_a = 24 μM actin + 5 % FLN.

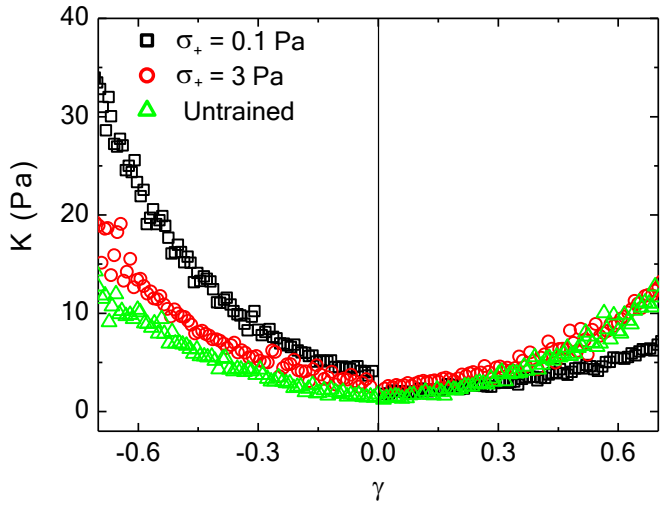

Figure S2 Bringing a maximally trained sample back to the untrained state. Raw data for the shear modulus K as a function of applied strain γ for two training stress values (indicated in the figure legend) applied in the opposite direction to the initial training as mentioned in Fig.2d in the main text. This plot indicates that, starting with a highly asymmetric state (large memory), it is possible to bring back the sample to a state that is close to the untrained (no memory) state by applying suitable opposing stress pulses.

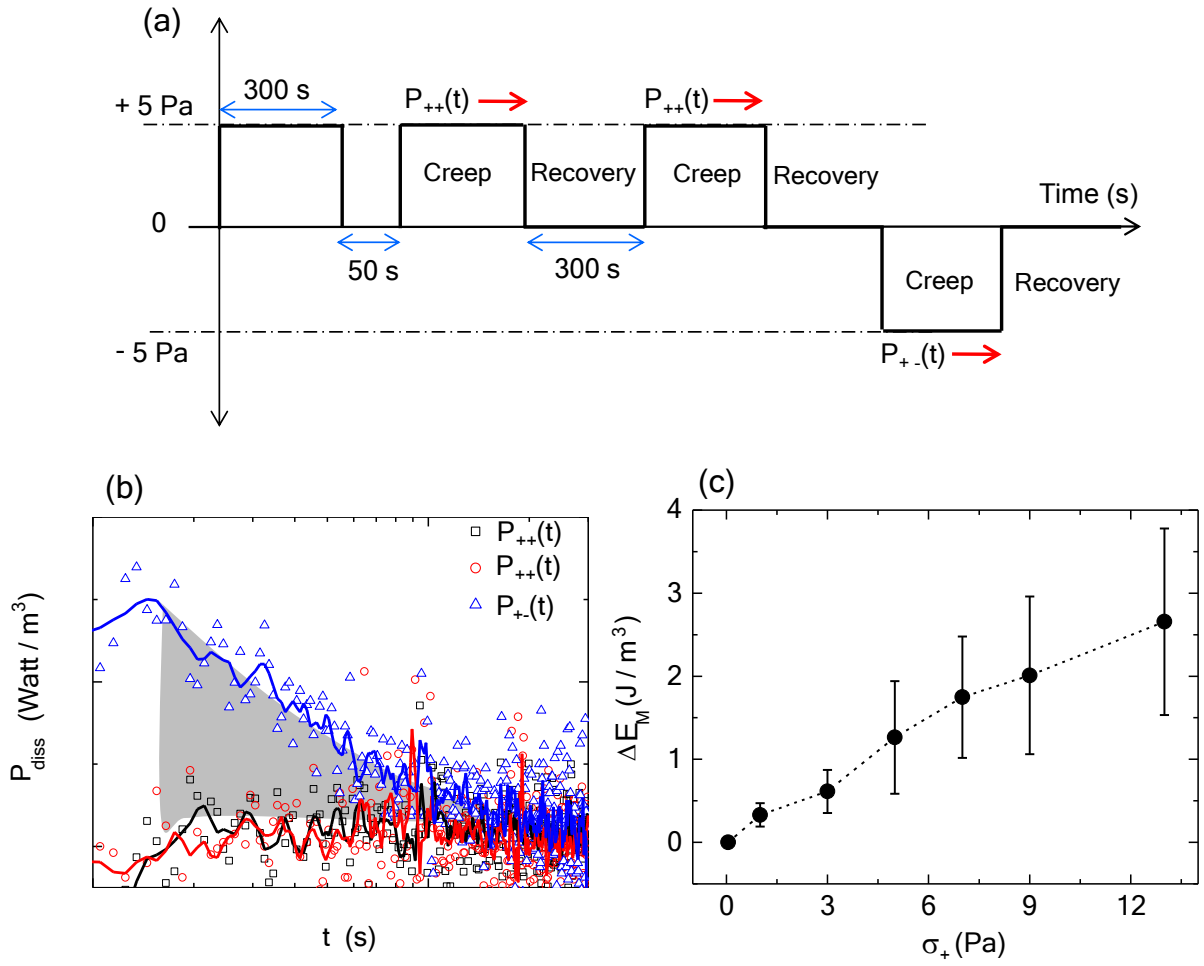

Figure S3 Absolute energy dissipation in re-writing a memory from creep and recovery measurements. **a**, Schematic of the protocol: An untrained sample (c_a = 24 μM actin + 5 % FLN) is first trained by σ_+ = 5 Pa stress in the positive direction for 300 s. After waiting for 300 s, a stress of magnitude 5 Pa is again is applied for 300 s and then the stress is switched off (σ = 0 Pa) for 300 s. We estimate the shear rate as a function of time by numerically differentiating the strain data during both creep ($\dot{\gamma}_c(t)$) and recovery ($\dot{\gamma}_r(t)$) as indicated in Fig.3 in the main text. The difference shear rate is measured by $\Delta\dot{\gamma}(t) = \dot{\gamma}_c(t) - \dot{\gamma}_r(t)$. The quantity $\sigma\Delta\dot{\gamma}(t)$, gives the instantaneous power dissipation. $P_{++}(t)$ and $P_{+-}(t)$ represent the power dissipation when the creep stress direction is same or opposite to the training direction, respectively. **b**, $P_{++}(t)$ and $P_{+-}(t)$ as a function of time. The integrated area between $P_{+-}(t)$ and $P_{++}(t)$ indicated by the gray region gives the total dissipated energy ΔE_M in re-writing a memory. The symbols represent the raw data and the lines represent the spline curve (obtained by 5 points moving averaging). **c**, ΔE_M as a function of D.C. stress pulse magnitude. The error bars represent the standard deviation of the fluctuations in power vs the time data in (**c**).

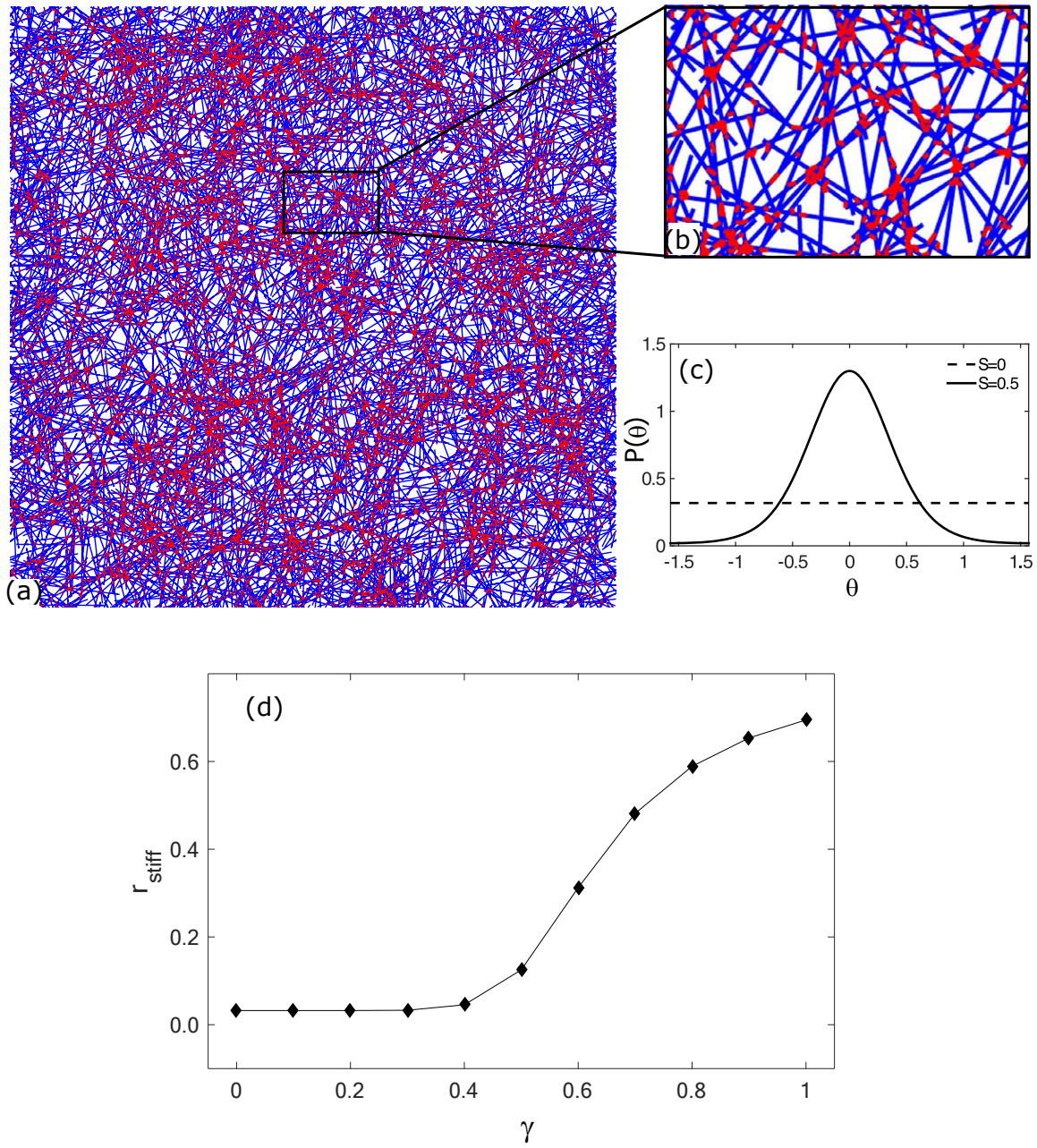

Figure S4 Example of a semiflexible network in two dimensions. **a**, Actin filaments are in blue and the filamin cross-linkers in red. **b**, The close-up view of the cross-linking of filaments shown in (**a**). **c**, The orientation distribution of filaments in the nematic network. Here, the orientation angle θ of a filament is measured w.r.t. the nematic director of the network. **d**, Fraction of filamin molecules getting stiffened when such network is strained. We see that, beyond a strain of ~ 0.4, the number of stiffened filamin molecules increases rapidly indicating that constitutive non-linearity takes over the geometric non-linearity at large strain values.

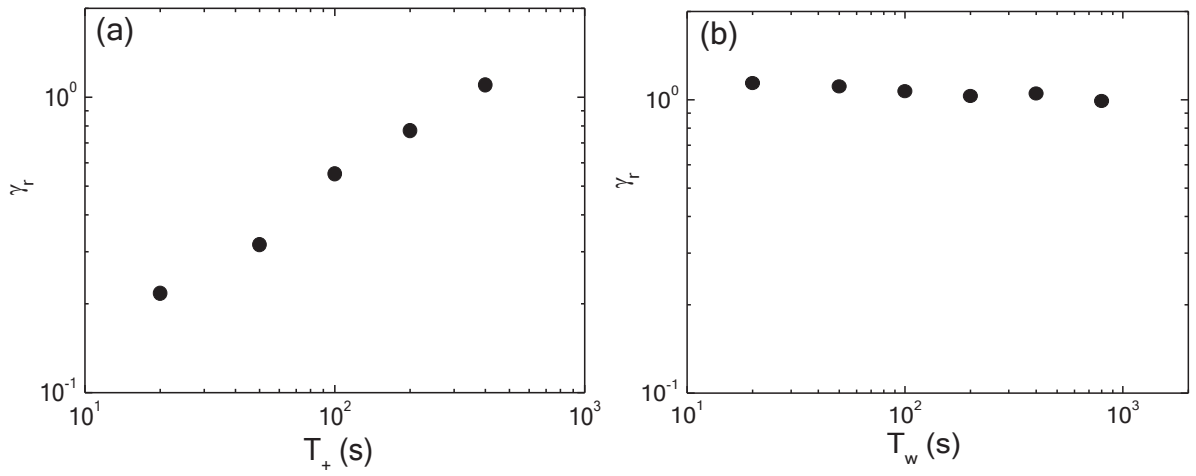

Figure S5 Evolution of residual strain as a function of training and waiting time. **a**, An untrained sample (c_a = 24 μM actin + 5 % FLN) is trained by σ_+ = 4 Pa stress in the positive direction with increasing training time T_+. The cumulative residual stain is shown as a function of T_+. **b**, The residual strain as a function of waiting time. The sample is initially trained with σ_+ = 4 Pa applied for T_+ = 300 s.

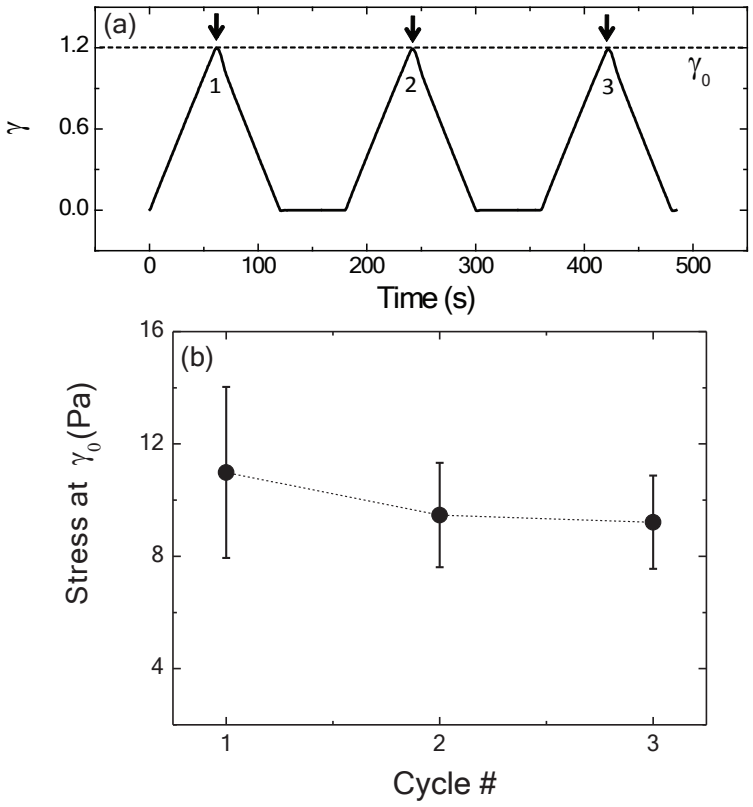

Figure S6 Variation of peak stress under cyclic loading. **a**, Schematic of the cyclic loading protocol. The strain ramp rate is 0.02 s^{-1} and the waiting time between two consecutive pulses is 60 s. The maximum strain position γ_0 is indicated by the arrows. **b**, Stress values at the position of maximum strain for three consecutive strain cycles as indicated in **a**. The error bars are estimated from the standard deviation of the stress values from three independent experiments on the same sample (c_a = 24 μM actin + 5 % FLN).

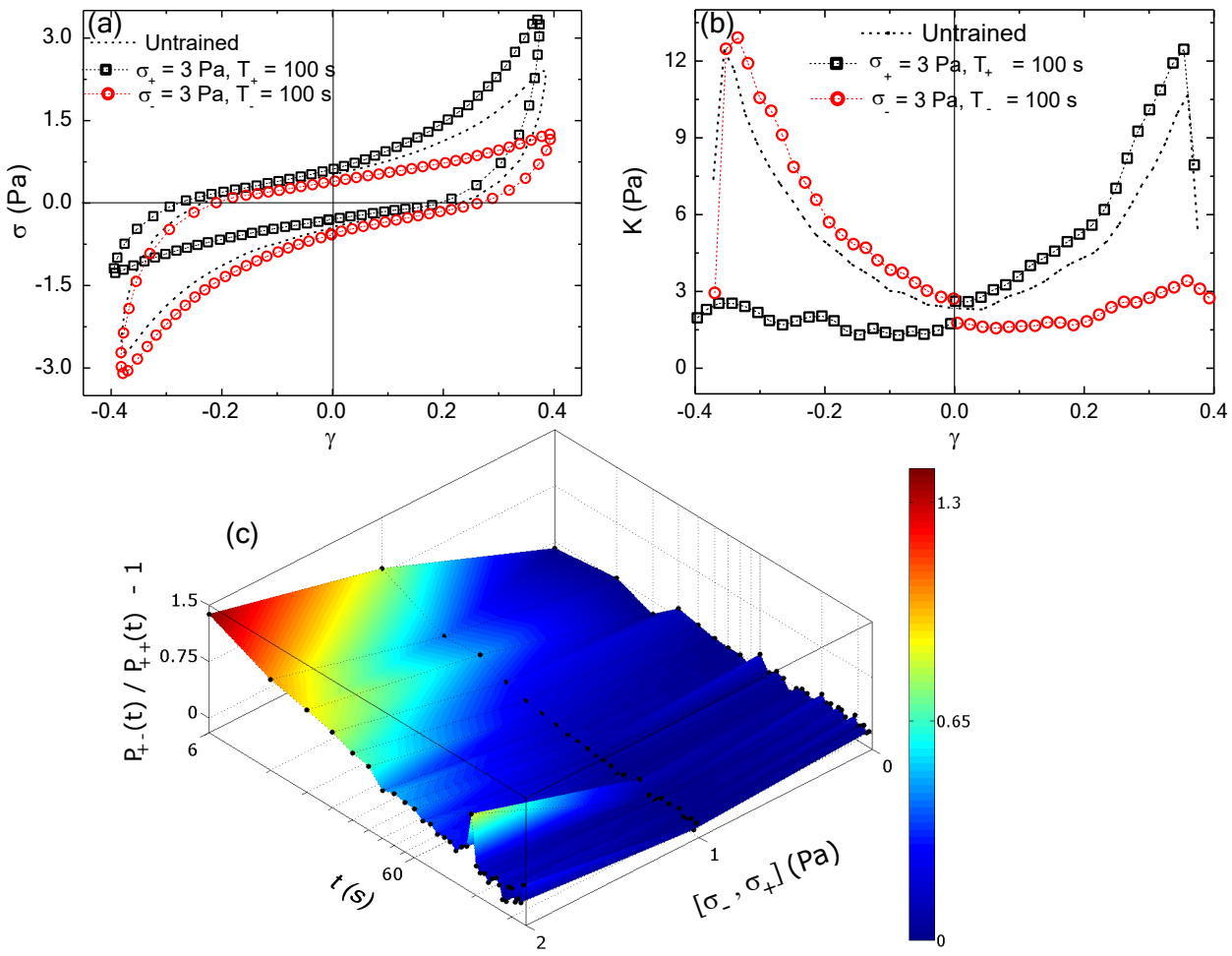

Figure S7 Memory effect in actin network cross-linked with a rigid cross-linker α-actinin. **a**, Lissajous plots (stress vs. strain) for an untrained, positively trained and negatively trained sample (c_a = 24 μM actin + 5 % α-actinin). The training stress magnitude and duration in different cases are shown in the figure legend. **b**, Shear modulus as a function of strain obtained from the Lissajous plots in panel **a**. **c**, Normalized time dependent power dissipation upon stress reversal, estimated by superposing a small A.C. component of stress on the D.C. stress pulses (see Fig.2d and Methods). The 3-D plot is generated by varying the magnitude [σ_+, σ_-] of D.C. pulses.

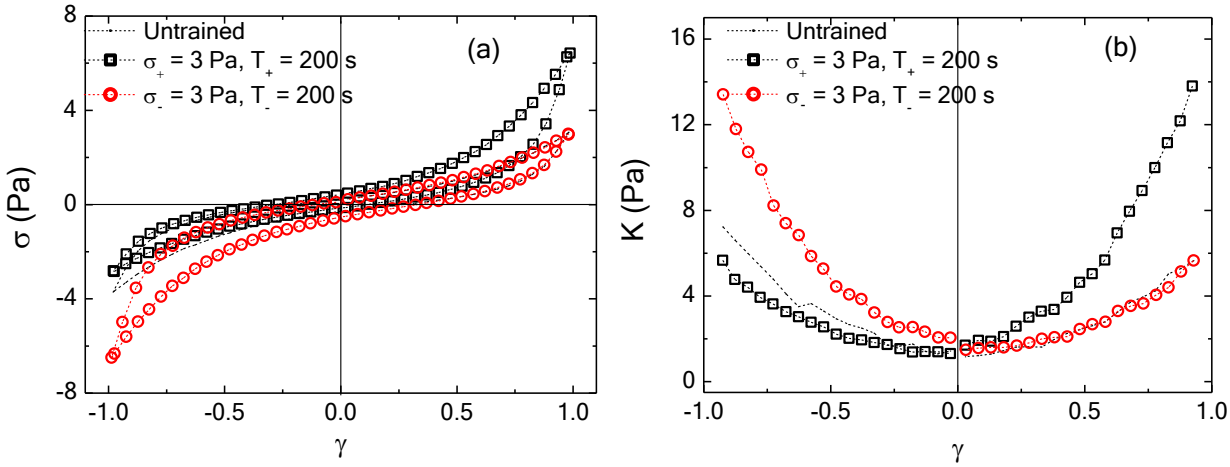

Figure S8 Memory effect in actin network probed by a cone and plate rheometer. **a**, Lissajous plots (stress vs. strain) for an untrained, positively trained and negatively trained sample (c_a = 24 μM actin + 2.5 % FLN). The training stress magnitudes and durations are indicated in the figure legend. **b**, Shear modulus as a function of strain obtained from the Lissajous plots in panel **a**. These results are similar to that obtained using a parallel plate rheometer. Here, the diameter of the cone is 20 mm and the cone angle is 1°.

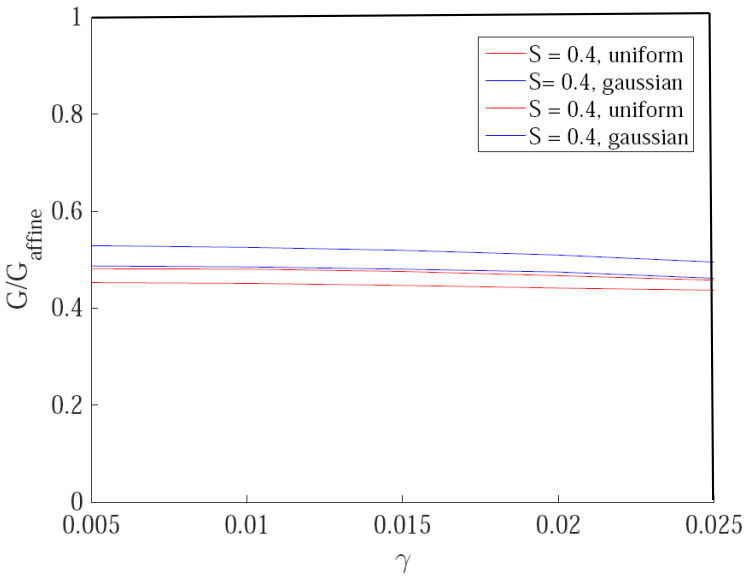

Figure S9 Linear modulus versus strain for nematic networks prepared with different forms of their orientational order. The (red) uniform networks have step orientational distributions so that all angles within $\Delta\theta = \pi/3$ the nematic director are equally probable and all other orientations are disallowed. The (blue) Gaussian distributions ($\sigma^2 = \pi/8$) replace the step distribution with a Gaussian one, as used in all simulations reported in the manuscript. The comparisons are done for two different samples (one pair of curves for each) to also study the sample to sample variations. The difference in modulus between these networks is small in all cases.